Detection efficiency characteristics of free-running InGaAs/InP single photon detector using passive quenching active reset IC*

Fu Zheng(郑福)[1,2], Chao Wang(王超)[1,3], Zhi-Bin Sun(孙志斌)[1], and Guang-Jie Zhai(翟光杰)[1,†]

[1] *Key Laboratory of Electronics and Information Technology for Space Systems, National Space Science Center, Chinese Academy of Sciences, Beijing* 100190, *China*

[2] *University of Chinese Academy of Sciences, Beijing* 100049, *China*

[3] *College of Physics, Beijing Institute of Technology, Beijing* 100081, *China*

(Received 30 June 2015; revised manuscript received 10 September 2015; published online 1 December 2015)

InGaAs/InP avalanche photodiodes (APD) are rarely used in a free-running regime for near-infrared single photon detection. In order to overcome the detrimental afterpulsing, we demonstrate a passive quenching active reset integrated circuit. Taking advantage of the inherent fast passive quenching process and active reset to reduce reset time, the integrated circuit is useful for reducing afterpulses and is also area-efficient. We investigate the free-running single photon detector's afterpulsing effect, de-trapping time, dark count rate, and photon detection efficiency, and also compare with gated regime operation. After correction for deadtime and afterpulse, we find that the passive quenching active reset free-running single photon detector's performance is consistent with gated operation.

Keywords: single photon detector, free-running, passive quenching, active reset

PACS: 03.67.Hk, 85.40.−e, 42.79.Qx **DOI:** 10.1088/1674-1056/25/1/010306

1. Introduction

High-performance InGaAs/InP single-photon avalanche diodes (SPADs) in near-infrared range between 1.0–1.7 μm are required in many fields, such as quantum key distribution (QKD),[1] time-of-flight (TOF) measurements, fluorescence lifetime imaging (FLIM), and fluorescence correlation spectroscopy (FCS).[2] For single photon detection, an SPAD is usually dc biased a few volts below its breakdown voltage, and is periodically pulse biased above breakdown voltage for a very short time, which is called gated operation.[3] This requires the synchronization between the gates and the coming photons, thus limits its application.[4] For a variety of situations, photons do not come in a known pattern, where the SPADs are required to operate in the free-running regime.[5]

Due to its relatively narrow bandgap ($E_g = 0.75$ eV for $In_{0.53}Ga_{0.47}As$), it usually exhibits more dark counts.[2] Moreover, carriers produced by previous avalanches, can be trapped by the deep levels in the multiplication layer. They can release at a later time and lead to another avalanche. Therefore, in practice, we must apply a very long deadtime, during which the SPAD is biased blow its breakdown voltage, and wait for these carriers to release.[6] This severely limits detection rate. On the other hand, the more carriers an avalanche produces, the more likely an afterpulse happens; and the number of carriers is proportional to avalanche duration. Consequently, to reduce the afterpulsing phenomena, one needs to quench the avalanche rapidly, as soon as it is sensed.[7]

Many techniques have been developed to achieve this goal. With the traditional passive quenching method, the passive reset stage takes a rather long time. Active quenching method actively quenches and resets SPAD, so the detection rate can be increased, and the deadtime is well controlled.[8] Integrated active quenching circuits[9,10] have been developed and also applied to the InGaAs/InP avalanche photodiodes (APD).[11,12] Discrete passive quenching active reset[13] is another method to reduce the afterpulsing effects, however it cannot be integrated with the APD. Negative feedback avalanche diodes (NFADs)[5,14] utilizing integrated resistors achieved good performance and are promising for array integration, but they only achieved passive quenching and reset.

In this paper, we demonstrate a passive quenching and active reset integrated circuit, and its operation principle. Then, we characterized the free-running InGaAs/InP single photon detector, using this integrated circuit, and extracted its afterpulsing probability, de-trapping time, dark count rate and photon detection rate through deadtime and afterpulse correction. At the same time, we compare the DCR and PDE between free-running regime and gated regime.

2. Passive quenching active reset IC

It is believed that, the intrinsic passive quenching is swift, while the passive reset takes a rather long time.[15] Here, we developed a passive quenching active reset integrated circuit

*Project supported by the National High Technology Research and Development Program of China (Grant No. 2013AA122902), the National Key Scientific Instrument and Equipment Development Project of China (Grant No. 2013YQ030595), and the National Natural Science Foundation of China (Grant Nos. 61274024 and 61474123).

†Corresponding author. E-mail: gjzhai@nssc.ac.cn

© 2016 Chinese Physical Society and IOP Publishing Ltd

with SMIC 0.18 μm CMOS process. The schematic is presented in Fig. 1(a), and the photomicrograph of the single cell of the circuit in Fig. 1(b). The pixel layout area is within 150 μm × 150 μm, easy for future array integration. As can be seen, the APD is connected with the IC at its anode, and it is biased with VBias at the cathode. The electronic model of the APD is based on the model in the article.[16] The parasitic resistor and capacitance is measured as described following the procedure in it.

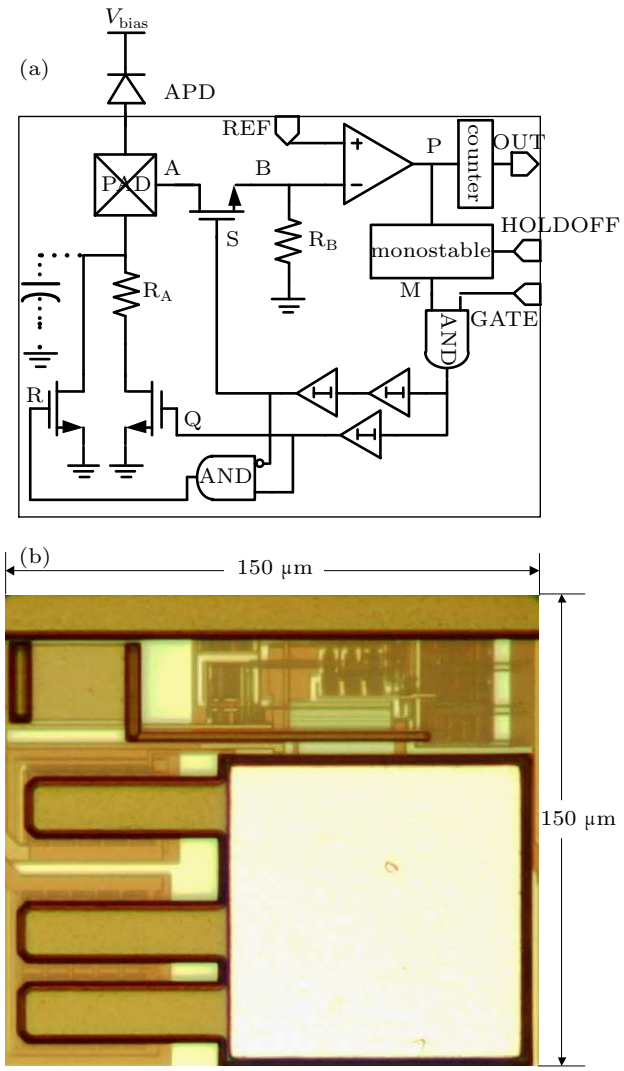


Fig. 1. (color online) (a) Schematic of the passive quenching active reset IC. (b) Photomicrograph of the single cell of the circuit.

The operation principle is illustrated in Fig. 2. At quiescent state, the bias voltage is higher than its breakdown voltage; and when triggered the avalanche current flows into R_A and R_B, and raises the voltage A. As soon as the voltage A bypasses the REF voltage, which is provided outside the pixel, the fast comparator turns low at node P. It triggers a monostable to provide a fixed deadtime, which is controlled outside the chip. The deadtime is adjustable from 10 ns to 500 μs allowing for desired optimization of the trade-off between peak count rates and low afterpulsing. The falling edge passes through an AND gate and a small delay to node Q, switching the quench transistor M_Q off swiftly. As a result, the current path is cut off. Then it charges the parasitic capacitor and the voltage continues to grow until the voltage across the APD drops near the breakdown voltage. This achieves passive quenching. The monostable output also transmits to node S through a relatively long delay, thus switching the transistor M_S off. The comparator input voltage B drops quickly, and the comparator turns high again. After the deadtime ends, the monostable output turns high, and transmits to node Q and S to close the switches M_Q and M_S successively. The time difference of signal Q and S, caused by different path delays, produces a reset pulse. It closes M_R, which rapidly decreases the voltage A to ground. This achieves active reset. At this moment, the single photon detector is back to the quiescent state and ready for another photon. The output pulse can either be sent outside the chip or be sent to an 8-bit linear feedback shift register (LFSR) to be counted. Gate signals can be applied to the chip through the GATE pin, which we called the gated mode. Although it differs from the normal gated operation slightly, where at the gated-off period the APD is biased below breakdown voltage, in this scenario the APD is cut off from the circuit, where it still cannot trigger avalanches. Consequently, we still consider this operation as the gated operation and further compared the performance in detail below. The measured anode signal waveform is shown at overbias of 0.9 V and deadtime of 1 μs in Fig. 3, which is consistent with the analysis. It can been seen in Fig. 3, the resistive passive quenching time is about 150 ns; the passive charging time is 350 ns. As a result, the total quenching time is about 500 ns. While the fast reset stage takes about 30 ns.

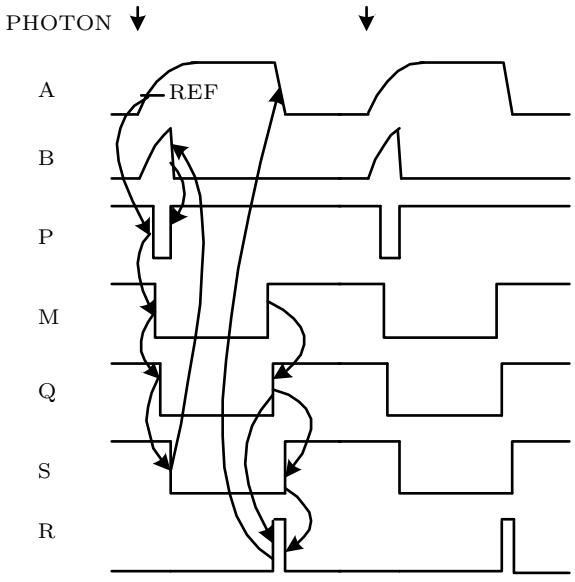


Fig. 2. Waveform illustration of the passive quenching active reset IC.

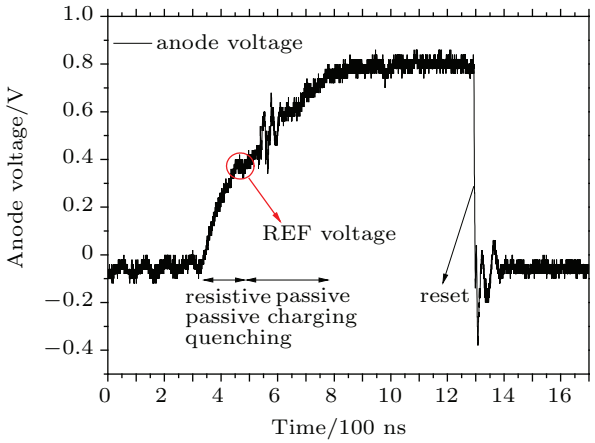


Fig. 3. Measured waveform at the anode of APD at overbias of 0.9 V and deadtime of 1 μs.

3. Free-running single photon detector performance

With this passive quenching active reset integrated circuit, we can characterize the free-running single photon detector performance, such as dark count rate (DCR), photon detection efficiency (PDE), and afterpulsing probability (AP). We utilized the APD, fabricated in separate absorption graded charge multiplication (SAGCM) structure.[17] The 1550 nm pulsed laser (id300, id Quantique) is fed to the APD through a single mode fibre, and attenuated to 0.1 photon/pulse. The APD is cooled to 219 K by a Peltier cooler (RMT Ltd, 2MDX04-138-0816).

When the laser is switched off, the APD's internal thermally generated carriers, direct band-to-band tunneling (BBT) and trap-assisted tunneling (TAT) can also contribute to count rates, which is dark count rate. The photon detection efficiency is the product of external optical coupling efficiency on the photodiode, the electric carriers generation probability by absorbed photons and the avalanche triggering probability by the photo-generated carriers.[18] Afterpulsing probability is the probability that trapped charge carriers created during a previous avalanche release and induce spurious avalanches.

3.1. Afterpulsing measurement

We applied a deadtime to relieve the afterpulsing effect. The double-pulse method[19] is adopted to extract the afterpulsing probability by applying a train of short pulse of 100 ns to the GATE pad. By tuning the time difference between light gates and subsequent dark counts, we can obtain the afterpulsing probability $P_{\rm ap}$ with

$$P_{\rm ap} = \frac{C_{\rm t2} - C_{\rm d2}}{C_{\rm t1}}, \tag{1}$$

where $C_{\rm t1}$ and $C_{\rm t2}$ are the total counts in the first light gates and in subsequent dark gates respectively when first gates are illuminated with 100 photons/pulse ensuring avalanche; $C_{\rm d2}$ is the dark counts in subsequent dark gates when the laser is turned off, which is almost the same as in the first gates.

We plot afterpulsing probability dependence on deadtime at different bias voltages in Fig. 4. As can be seen, the afterpulsing probability decreases with deadtime following exponential pattern. With the bias voltage increasing, the avalanche current becomes bigger. As a result, the afterpulsing probability grows with the bias voltage.

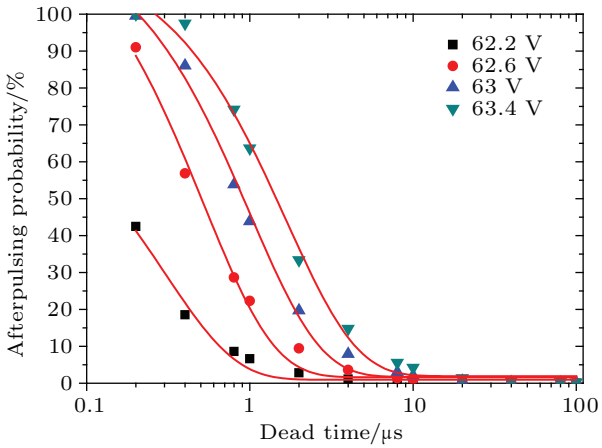


Fig. 4. Afterpulsing probability dependence on deadtime at different bias voltages and their exponential fit.

It indicates that the deep levels in the APD can be modeled as a single type of trap.[19] Therefore, we can extract its de-trapping time parameter through the procedure described in Ref. [20].

First of all, we can express the total measured count rate $R_{\rm tm}$ as

$$R_{\rm tm} = R_{\rm di} + R_{\rm pi} + R_{\rm ap}(t), \tag{2}$$

where $R_{\rm di}$ is the intrinsic (afterpulse-free) dark count rate, $R_{\rm pi}$ is the intrinsic (afterpulse-free) photon count rate, and $R_{\rm ap}(t)$ is the time-dependent afterpulse count rate. Meanwhile, by performing ensemble average, the observed afterpulsing $R_{\rm ap}$ can be written as

$$\begin{aligned} R_{\rm ap} &= \langle R_{\rm ap}(t)\rangle = \langle C_0 \exp[-(t+T_{\rm d})/\tau_{\rm tr}]\rangle \\ &= C_0\langle \exp(-t/\tau_{\rm tr})\rangle \exp(-T_{\rm d}/\tau_{\rm tr}) \\ &= C\exp(-T_{\rm d}/\tau_{\rm tr}), \end{aligned} \tag{3}$$

where we denote $C \equiv C_0\langle \exp(-t/\tau_{\rm tr})\rangle$, C_0 is defined as a prefactor depending on the current flowing through the APD, and $\tau_{\rm tr}$ and $T_{\rm d}$ are deep level de-trapping time and the deadtime, respectively. With this formula, we can fit the experiment data to extract $\tau_{\rm tr}$ and C_0. Then, we obtain the experimental data of raw count rate versus photon flux at different deadtime at 62.4 V bias voltage, as shown in Fig. 5. Finally, we use the count rate at three different deadtimes to form an equation group, and thus C, $\tau_{\rm tr}$, and $R_{\rm pi} + R_{\rm di}$ are calculated. Besides, we obtain one set of these three parameters at every photon flux, as shown in Fig. 6.

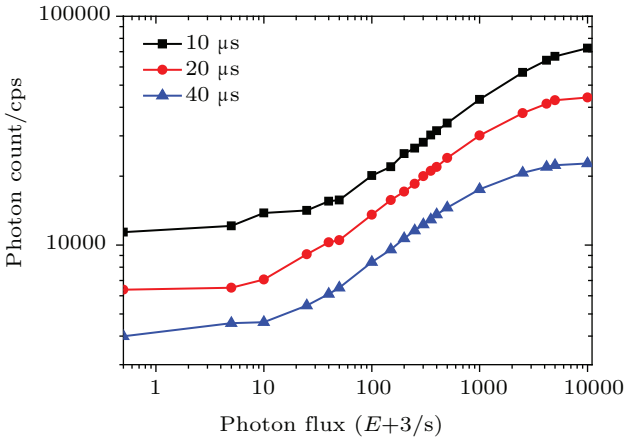


Fig. 5. Raw count rate versus photon flux at 62.4 V bias voltage at 10 μs, 20 μs, 40 μs deadtime. The cps is for counts per second.

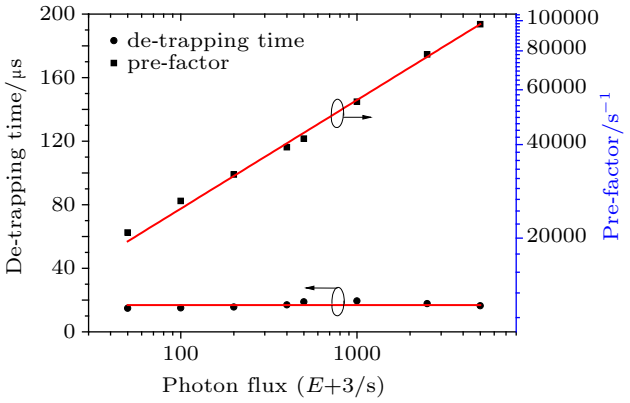


Fig. 6. Extracted pre-factor C (square, right axis) and de-trapping time τ_{tr} (circle, left axis) versus photon flux.

Here, we can see that, the pre-factor C is almost linear with the photon flux in this log–log plot. It confirms that C_0 is proportional to avalanche current. The de-trapping time does not vary much at different photon flux, indicating that the de-trapping time constant is about 16.8 μs.

3.2. Dark count rate and photon detection efficiency

In order to prevent afterpulsing, the free-running regime applies long deadtime while photons come randomly. Thus, the device is nonlinear and its performance depends on deadtime and afterpulses. We can perform deadtime correction[21] and afterpulse correction[14] to the count rates and obtain intrinsic DCR and PDE. Also, we performed the gated operation by applying 100-ns-width pulse to the GATE pad and compared the performance between free-running regime and gated regime. By scanning the laser-to-gate delay with a step of 5 ns, we obtain the photon counts distribution. We normalize the counts and obtain the effective gate width of 95 ns as shown in Fig. 7.

We measured the dark count rate with laser off as a function of bias voltage for different deadtimes. Depending on deadtime, the laser repetition frequency is $f_{\text{laser}} = 1/T_{\text{d}}$. The intrinsic dark count rate R_{di} for deadtime and afterpulse correction is expressed as

$$R_{\text{di}} = \frac{R_{\text{dm}}}{(1 - R_{\text{dm}} T_{\text{d}})(1 + P_{\text{ap}})}, \tag{4}$$

where R_{dm} is the measured dark count rate and P_{ap} is the experimental afterpulsing probability in the above section.

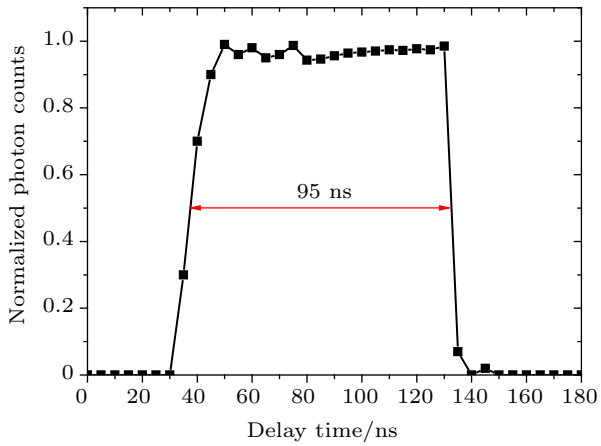


Fig. 7. Normalized photon counts versus laser-to-gate delay.

With the free-running DCR and gated DCR at different deadtime in Fig. 8, we can see that the DCR increases exponentially with bias voltage in both regimes. The free-running DCR is almost one order higher than the gated DCR. At different deadtimes, the gated DCR is almost the same; while the free-running DCR increases as the deadtime decreases, whereas they are still on the same order.

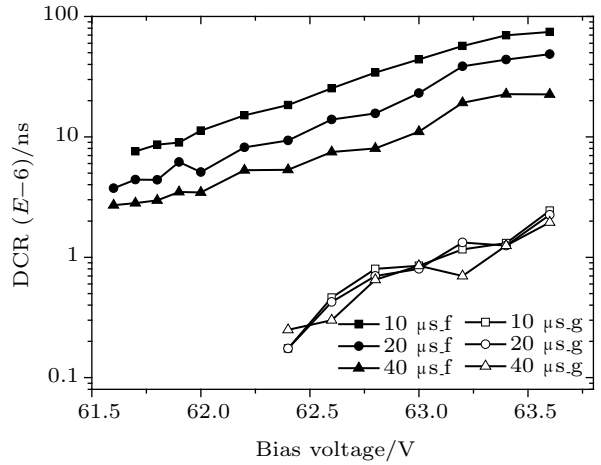


Fig. 8. Dark count rate versus bias voltage at different deadtimes with respect to gated regime and free-running regime. For example 10 μs_f and 10 μs_g denotes 10 μs deadtime free-running regime and gated regime, respectively.

By taking into account the deadtime and afterpulsing, the total measured counts R_{tm} is modeled as

$$R_{\text{tm}} = (\mu \eta_{\text{i}} + R_{\text{di}})(1 - R_{\text{tm}} T_{\text{d}})(1 + P_{\text{ap}}), \tag{5}$$

where $\eta_{\rm i}$ is the intrinsic photon detection efficiency, and μ is the photon number incident on the detector. Therefore, $\eta_{\rm i}$ can be derived from

$$\eta_{\rm i} = \frac{1}{\mu}\left(\frac{R_{\rm tm}}{(1-R_{\rm tm}T_{\rm d})(1+P_{\rm ap})} - R_{\rm di}\right). \quad (6)$$

The PDE of gated operation is calculated by[22]

$$\eta_{\rm g} = \frac{1}{\mu}\ln\left(\frac{1-P_{\rm d}}{1-P_{\rm t}}\right), \quad (7)$$

where $P_{\rm d}$ and $P_{\rm t}$ are the probabilities of dark counts and total counts, respectively.

In Fig. 9, the free-running PDE is consistent with the gated PDE at different deadtime, and both increase linearly with the bias voltage. However, at higher voltage, the free-running PDE begins to saturate, which is caused by the high DCR. Despite the little divergence, it is also concluded that PDE does not depend on the deadtime. The maximum free-running PDE is about 23%, where the DCR is 10^{-5} ns^{-1}.

Finally, the DCR versus PDE relationship at 20 μs deadtime is plotted in Fig. 10, where it follows almost the same exponential principle as the DCR versus bias voltage.

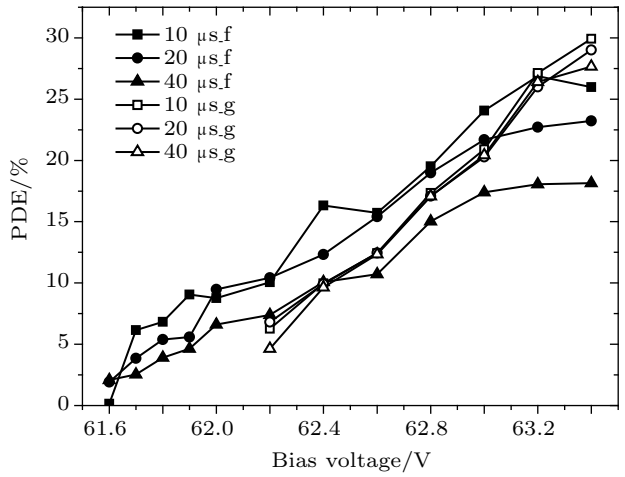


Fig. 9. Photon detection efficiency versus bias voltage at different deadtime with respect to gated regime and free-running regime. For example, 10 μs_f and 10 μs_g denotes 10 μs deadtime free-running regime and gated regime, respectively.

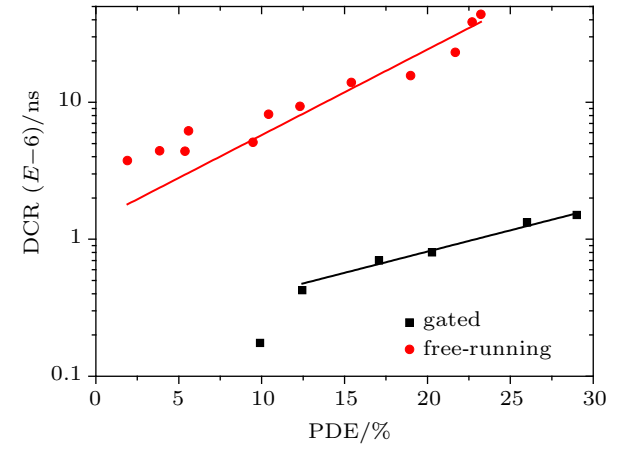


Fig. 10. (color online) Dark count rate versus photon detection efficiency at 20 μs deadtime.

4. Conclusion

In conclusion, we present a passive quenching active reset integrated circuit by taking advantage of the inherent fast passive quenching and active feedback reset. Combining this IC with an InGaAs/InP APD, we develop a free-running near-infrared single photon detector. Then, we comprehensively characterize the performance of this detector and compare with gated operation. We find that, the afterpulsing probability decreases with deadtime exponentially and the de-trapping time constant is 16.8 μs. The free-running DCR is higher than the gated DCR because of narrow band gap, and also follows the same principle. The free-running PDE is consistent with the gated PDE and does not depend on the deadtime. The maximum free-running PDE is about 23%, where the DCR is 10^{-5} ns^{-1}.

References

[1] Comandar L C, Frohlich B, Dynes J F, Sharpe A W, Lucamarini M, Yuan Z L, Penty R V and Shields A J 2015 *J. Appl. Phys.* **117** 083109
[2] Itzler M. A., Jiang X, Entwistle M, Slomkowski K, Tosi A, Acerbi F, Zappa F and Cova S 2011 *J. Mod. Opt.* **58** 174
[3] Liu Y, Wu Q L, Han Z F, Dai Y M and Guo G C 2010 *Chin. Phys. B* **19** 080308
[4] Zhang J, Thew R, Gautier J D, Gisin N and Zbinden H 2009 *IEEE J. Quantum Electron.* **45** 792
[5] Korzh B, Walenta N, Lunghi T, Gisin N and Zbinden H 2014 *Appl. Phys. Lett.* **104** 081108
[6] Warburton R E, Itzler M and Buller G S 2009 *Appl. Phys. Lett.* **94** 071116
[7] Ma H Q, Yang J H, Wei K J, Li R X and Zhu W 2014 *Chin. Phys. B* **23** 120308
[8] Cova S, Ghioni M, Lacaita A, Samori C and Zappa F 1996 *Appl. Opt.* 1996 **35** 1956
[9] Zappa F, Lotito A, Giudice A C and Cova S 2003 *IEEE J. Solid-State Circuits* **38** 1298
[10] Rochas A, Guillaume-Gentil C, Gautier J D, Pauchard A, Ribordy G, Zbinden H, Leblebici Y and Monat L 2007 *Proc. SPIE* **6583** 65830F
[11] Thew R T, Stucki D, Gautier J D and Zbinden H 2007 *Appl. Phys. Lett.* **91** 201114
[12] Zheng L X, Wu J, Zhang X C, Tu J H, Sun W F and Gao X J 2014 *Acta Phys. Sin.* **63** 104216 (in Chinese)
[13] Liu M, Hu C, Campbell J C, Pan Z and Tashima M M 2008 *IEEE J. Quantum Electron.* **44** 430
[14] Lunghi T, Barreiro C, Guinnard O, Houlmann R, Jiang X, Itzler M A and Zbinden H 2012 *J. Mod. Opt.* **59** 1481
[15] Gallivanoni A, Rech I and Ghioni M 2010 *IEEE Trans. Nuclear Science* **57** 3815
[16] Zappa F, Tosi A, Mora A D and Tisa S 2009 *Sensor. Actuat. A: Phys.* **153** 197
[17] Itzler M, Ben-Michael R, Hsu C F, Slomkowski K, Tosi A, Cova S, Zappa F and Ispasoiu R 2007 *J. Mod. Opt.* **54** 283
[18] Kang Y, Lu H X, Lo Y H, Bethune D S and Risk W P 2003 *Appl. Phys. Lett.* **83** 2955
[19] Jensen K, Hopman P, Duerr E K, Dauler E A, Donnelly J P, Groves S H, Mahoney L J, McIntosh K A, Molvar K M, Napoleone A, Oakley D C, Verghese S, Vineis C J and Younger R D 2006 *Appl. Phys. Lett.* **88** 133503
[20] Jiang X, Itzler M A, Ben-Michael R, Slomkowski K, Krainak M A, Wu S and Sun X 2008 *IEEE J. Quantum Electron.* **44** 3
[21] Chick S, Coath R, Sellahewa R, Turchetta R, Leitner T and Fenigstein A 2014 *IEEE Trans. Electron Dev.* **61** 2725
[22] Zheng F, Zhu G, Liu X F, Wang C, Sun Z B and Zhai G J 2015 *Optoelectron. Lett.* **11** 121